

Automated diagnostics of internal combustion engines using vibration simulation

Jian Chen^{1,2}, Robert Randall¹, Ningsheng Feng¹, Bart Peeters², Herman Van der Auweraer²

¹School of Mechanical and Manufacturing Engineering,
University of New South Wales, Sydney 2052 Australia

²LMS International, Interleuvenlaan 68, B-3001 Leuven, Belgium
{jian.chen1@unsw.edu.au}

Abstract

An Artificial Neural Network (ANN) based automated system was developed to diagnose a range of different faults in internal combustion (IC) engines, including combustion faults (misfire) and mechanical faults (piston slap and bearing knock). A critical issue with ANN applications is the network training, and it is neither feasible nor economical to expect to experience a sufficient number of different faults to obtain sufficient experimental results for the network training. Therefore, new simulation models, which can simulate combustion faults and mechanical faults in engines, were developed and are reported in this paper. In order to evaluate and update the simulation models, a small number of experiments with combustion faults and mechanical faults were carried out and the experimental vibration signals were studied first. The torsional vibration of the crankshaft and angular acceleration of the engine block were used to detect engine misfires. In contrast to the misfires, it has been demonstrated that an appropriate signal processing approach for diagnosis of the mechanical faults is envelope analysis of the vibration signals. The simulated signals were processed by the same signal processing techniques as the measurements and the selected features from the processed data were used to train the networks. The processed simulated data, with added random variations of the same order as in the measurements, provided sufficient data for the training of the ANNs. Finally, it was demonstrated that the networks trained on simulated data can efficiently detect both the combustion faults and mechanical faults in real tests and identify the location and severity of the faults as well.

1 Introduction

Most engine faults can be classified into two categories: combustion faults and mechanical faults. Misfire is a very common combustion fault for internal combustion (IC) engines and many works have been put forward to study vibration-signal-based misfire diagnosis. For the misfire diagnosis, the vibration based condition monitoring can be further divided into two types: one is based on the translational acceleration signals measured on the engine block [1-3], while the other is based on the torsional vibration signal of the crankshaft [4-8]. Owing to increased dynamic forces from excessive wear and larger clearances at the piston/cylinder wall interface and the journal/bearing interface, piston slap faults and big end bearing knock faults are considered to be two critical mechanical faults in engines. Many researchers have studied the mechanism of piston slap; in general, the aims of these works were focussed on the piston design, including the geometrical and lubrication aspects [9-12]. Meanwhile, many works have also been devoted to the dynamic response of the journal bearings with non-negligible clearance in the IC engine (slider-crank mechanism) [13-15]. But only a limited number of researchers have investigated the technology of using the measured vibration signals for the diagnosis/prognosis of piston slap faults [16, 17] and bearing knock faults [18].

Moreover, when these vibration-based techniques are applied in a real situation, the faults cannot automatically be diagnosed from the analysed vibration signals. Artificial Neural Network (ANN) techniques should be a potential solution to the problem of automated diagnostics of different faults in IC engines. Much research has shown that ANNs are a very efficient method to differentiate various faults of rotating machines [19-23]. A critical issue with ANN applications in machine condition monitoring is the network training, and

it is neither likely nor economical to experience a sufficient number of different actual faults, or generate them in seeded tests, to obtain sufficient experimental results for the network training. Simulation is proving to be a viable way of generating data to train neural networks to diagnose and make prognosis of faults in machines. Very little has been done on simulation of faults in IC engines, primarily limited to combustion faults, which had been shown to affect the torsional vibrations of the crankshaft. An example was given for simulation of misfire in a large 20-cylinder diesel engine [8].

In this paper an ANN based system was developed to automatically diagnose a range of different faults in IC engines, including combustion faults (misfire) and mechanical faults (piston slap and bearing knock). In order to obtain sufficient data for the training of ANNs, simulation models were developed in the simulation software packages, to simulate a range of combustion faults and mechanical faults in engines. The simulation models were validated and updated by a series of experiments. Advanced digital signal processing techniques were applied on the experimental and simulated vibration signals. The torsional vibration of the crankshaft and the roll rotation of the engine block were used for the diagnostics of misfires. Because the vibration signals from piston slap faults are typical second order cyclostationary signals, envelope analysis was used to process the vibration signals for their diagnosis. The input vectors of the ANNs were extracted/selected features from the processed signals. The automated diagnostic system consists of three stages: fault detection, fault localization and severity identification. The ANN systems were trained entirely by the simulated data and tested using real experimental cases.

2 Experimental setup

A series of vibration signals in normal condition and with a range of faults were recorded on a Toyota four cylinder gasoline engine at UNSW. Five accelerometers were used to record the vibration on the surface of the engine block, and their layout (limited by accessible mounting bosses) is shown in Figure 1. Two proximity transducers were used to pick up a once-per-rev tacho signal and a ring gear encoder signal (tooth passage). The cylinder pressure was measured by a special spark plug with integrated cylinder pressure sensor. Three constant speed conditions were selected for the engine tests: 1500rpm, 2000rpm and 3000rpm. For each speed, there were three different load conditions: 50Nm, 80Nm, 110Nm. Two stages of mechanical fault were seeded into the test engine for the two fault types. Cylinder 1 was bored to get three times normal clearance (1st stage piston slap fault) and six times normal clearance (2nd stage piston slap fault). After that, the crank journal of cylinder 2 was ground to increase the big end bearing clearance to two times normal clearance (1st stage bearing knock fault) and four times normal clearance (2nd stage bearing knock fault).

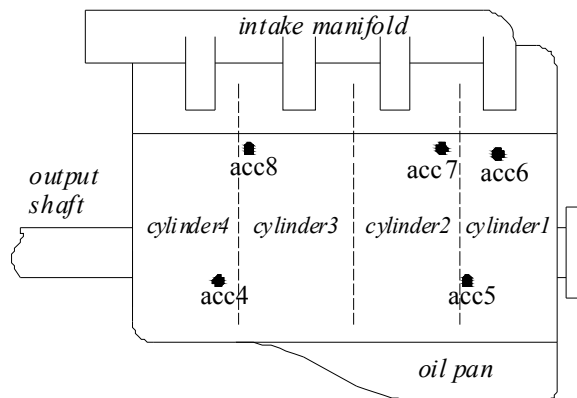


Figure 1: Accelerometer layout

3 Experimental and simulation results from combustion faults

The torsional vibration signal is obtained by phase demodulation of the ring gear encoder signal. The unwrapped phase angle demodulated from the first harmonic of the encoder signal represents the torsional vibration signal of the crankshaft when divided by the number of teeth (120) to get it in terms of the angular

displacement of the shaft. Next the angular displacement of the shaft was differentiated to get the angular velocity. Finally the angular velocity was synchronously averaged for pairs of cycles (to check the validity of the average). The roll rotation of the engine block was analysed from the averaged difference of a pair of translational accelerations. The signals from accelerometers 5 and 7 were subtracted to remove the translational components. The subtraction results were divided by the distance between the two measurement points to calculate the pseudo angular acceleration of the block. It is called pseudo angular acceleration because the measurement points are not in line with the centre of gravity (CG) of the engine (their line is not parallel to the principal axis of the engine either) and the calculated angular acceleration is mixed with other rotational motions. This approach was taken because the position of the CG was not known exactly.

In order to simulate the misfire phenomena under various speed/load conditions, the most critical variable, cylinder pressure, should first be calculated. The chamber pressures can be calculated by using Wiebe's functions, for which the details for this engine can be obtained from the former work [24, 25]. The calculated chamber pressure is also a critical variable for the simulation models of mechanical faults in the following section. From the mechanical viewpoint, to run and validate these models, the parameters of the engine components should be measured or calculated first. Besides the inertia properties of the engine components, the inertia properties of the whole engine and the characteristics of the engine supports are important parameters for the simulation of pseudo angular accelerations. Vibration based methods have been used to identify these parameters, including the mass line method and the modal property method. The details of the measurements of these parameters can be obtained from the former work [26].

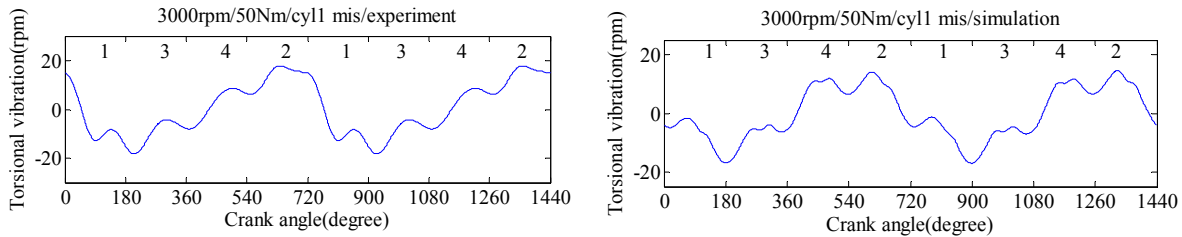


Figure 2: Experimental and simulated torsional vibration for the misfires in the cylinder 1

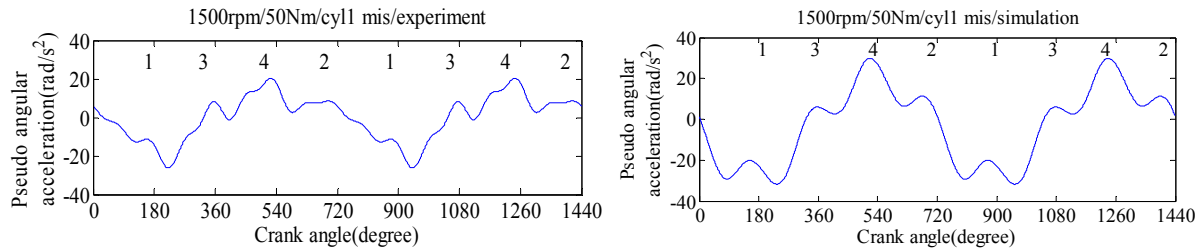


Figure 3: Experimental and simulated pseudo angular accelerations of the engine block for the misfires in cylinder 1

Both the torsional vibration of the crankshaft and pseudo angular accelerations were simulated in LMS' AMESim. For the simulation of torsional vibration of the crankshaft, even though the crankshaft of the experimental engine is quite rigid, the connections between the individual cylinders were modelled as rotary spring and damper sub-models and the effects of torsional modes were included in the modelling (though found to be negligible). Therefore the simulated torsional vibration model can be easily extended to larger engines. An example of experimental and simulated torsional vibration with misfires happening in cylinder 1 at 3000rpm/50Nm is shown in Figure 2. An example of experimental and simulated pseudo angular accelerations with misfires happening in cylinder 1 at 1500rpm/50Nm is shown in Figure 3. It will be found that the simulated waveforms for the misfires showed a relatively good correspondence with those from the experiments.

In order to extract/select features for input to the ANNs, inspired by the pattern recognition research of Desbazeille et al. [8], polar diagrams of the Fourier coefficients of the processed vibration waveforms were

employed to interpret the harmonics of the waveform patterns. It was found that the torsional vibration signal is easier and more straightforward to interpret than the block angular acceleration signal for misfire diagnosis, though this would only apply for a rigid crankshaft. However, based on both measured torsional vibration and pseudo angular acceleration of the engine block, it was not difficult to reach the conclusion that the ratio of the amplitudes of the 1st and 4th harmonics could be used for the misfire detection, and the phase of the 1st harmonic could also be used for the misfire localization

4 Experimental and simulation results for mechanical faults

4.1 Envelope analysis

The vibration signals from both mechanical faults (piston slap and bearing knock) are typical second order cyclostationary signals, so an appropriate signal processing approach for their diagnosis is envelope analysis. The “fast kurtogram” developed by Antoni [27] can be used as an aid in selecting the optimum demodulation band before performing envelope analysis. Two examples of the results from the “kurtogram” for the piston slap faults are shown in Figure 4, where the brown area indicates the most impulsive frequency range.

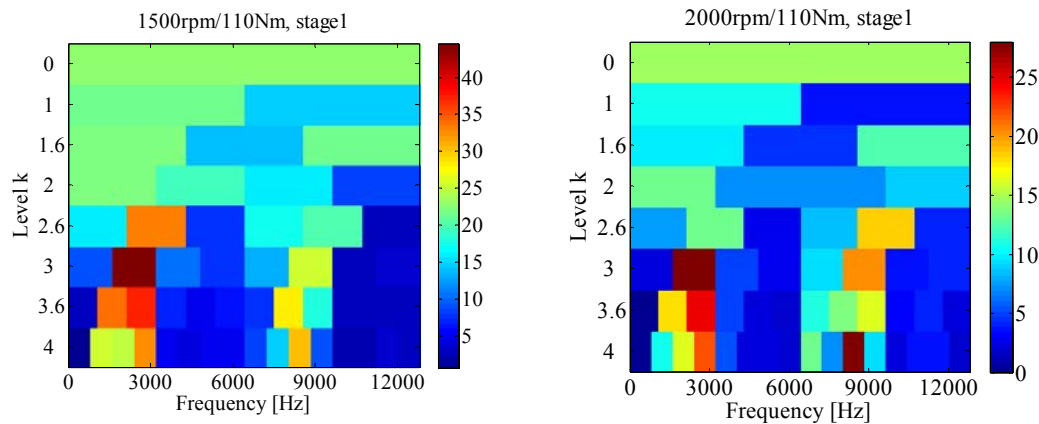


Figure 4: Results from “kurtogram” for piston slap faults

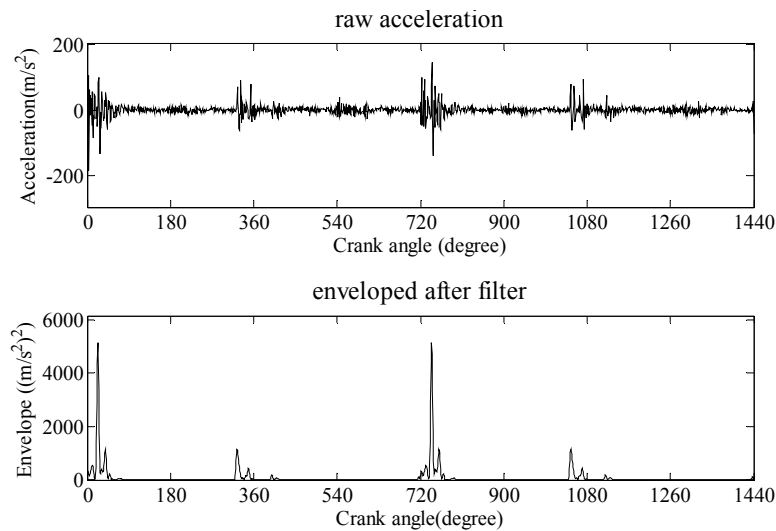


Figure 5: Raw acceleration signal and squared envelope after filtering for the 2nd stage piston slap fault at 2000rpm/110Nm

In order to have a fixed basis for comparison, for all cases, the frequency bands were adjusted and a common frequency band was found (somewhat broader than those in the two kurtograms). The most important premise of the adjustment was that there is no significant feature change or loss in the subsequent

Fourier analysis of the envelope. Examples of the raw signals and filtered squared envelopes with a piston slap fault are shown in Figure 5. It can be seen that the diagnostic information for mechanical faults became more obvious after the envelope analysis. In particular it was also found that, for low speed conditions, the bearing knock faults are not easy to detect from the change in the squared envelope signal. Actually, it was found that at lower speeds, the intensities of the raw accelerations with bearing knock faults have only a small increase from those in normal conditions, but at higher speed (3000rpm), the increases were very obvious (the change in audible sound was also quite clear at higher speed during the experiments).

Due to the transient characteristics, the diagnosis of mechanical faults is more complicated than that for misfires and more harmonics of the Fourier coefficients (the first forty harmonics) should be taken into account. However, the candidate features have different sensitivities to the different conditions of the engine and only some of them were found useful for the pattern recognition of the mechanical faults. Moreover, it requires a large amount of computing resources if all features are to be input into the ANNs. Thus it is important to select the optimal features to input into the ANNs, especially for the amplitude feature selection. A GA algorithm [28] was applied to find the best amplitude features for the diagnostics of piston slap or bearing knock faults. In order to find the best phase features to identify which cylinder has a piston slap or bearing knock fault, the scattering properties of the phases of the first 20 harmonics were studied. It was found that the phases of higher harmonics are more scattered and the most useful information to identify the localization of mechanical faults was contained in the lower harmonics. Therefore, the best phase features were selected from the first ten harmonics. The detail of the feature selection for the mechanical fault diagnosis can be obtained from the former work [29].

4.2 Simulation of piston slap faults

During the engine operation, when the resultant transverse force exerted by the connecting rod changes direction, the piston leaves the side of the inner wall it was previously held against, and moves to the other side of the inner wall. If the lateral acceleration of the piston (induced by the transverse force) is big enough and the interval until the next time the force direction changes is long enough, the piston will move across the clearance and collide with the opposite side of the inner wall. The impacts caused by oversize clearance will then excite more intensive vibration of the engine block. The side-thrust force F_{y11} can be solved by Equation (1).

$$F_{y11} = \frac{(F_g - F_{iz}) \frac{R}{b} \sin \theta}{\sqrt{1 + (\frac{R}{b} \sin \theta)^2}}$$

$$= \frac{[F_g - m_p R \omega^2 (\cos \theta + \frac{R}{b} \cos 2\theta)] \frac{R}{b} \sin \theta}{\sqrt{1 + (\frac{R}{b} \sin \theta)^2}} \quad (1)$$

where R is the crank radius. b is the centre-to-centre connecting rod length. θ is the crank angle. ω is the rotating speed of the crankshaft. F_g is the combustion force and F_{iz} is the axial inertia force of the piston. m_p is the mass of the piston.

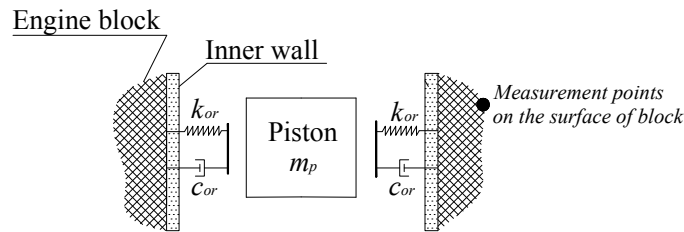


Figure 6. Interaction model between the piston and inner wall

Similar to the models from [10] and [12], a model was developed to represent the dynamic characteristics of the piston and inner wall when there is an oversized clearance. In this model, the piston and inner wall were modelled as lumped masses. The effect of the piston rings and lubricating oil was modelled as a viscous damper and spring between the piston and inner wall (shown in Figure 6). The spring and damper are of fixed length independent of the clearance, so that they only come into play when the piston is close to the inner wall. The end of the spring/damper was fixed to the engine block. When the piston contacts the surface of the inner wall, the dynamic model enters a boundary condition (dry contact) and the effects of the spring and damper are negligible. The impact force caused by the elastic contact is solved using Hertz theory.

A model was built in the Motion module of LMS' Virtual.Lab for the simulation of piston slap faults. Because it had been found that the useful information for the piston slap fault diagnosis lies in the processed envelope signals, the simulations only need to produce the correct envelope signals rather than raw acceleration signals. An example of the comparison between the experimental envelope and simulated with piston slap fault at 2000rpm/50Nm is shown in Figure 7. It can be seen the simulated envelope signals have good agreement with experiment.

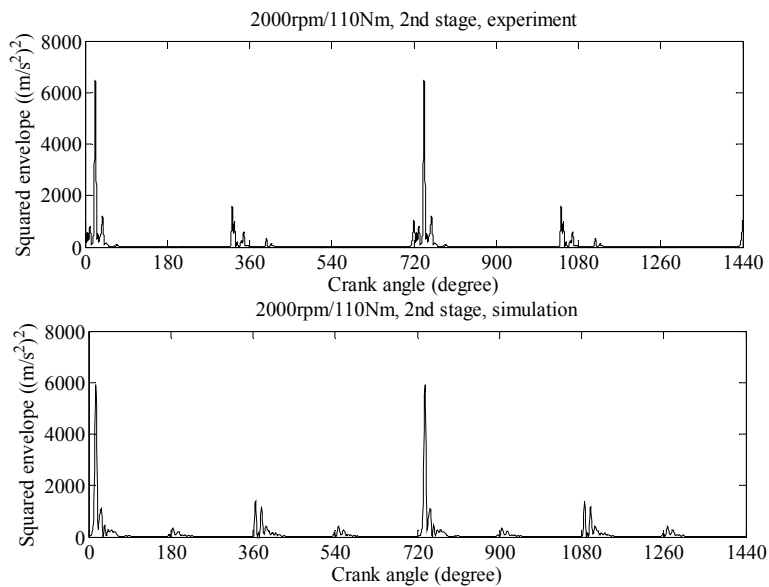


Figure 7. Simulated and experimental envelope signals with 2nd stage piston slap fault

4.3 Simulation of bearing knock faults

In the simulation system of bearing knock faults, by adjusting the clearance, the impact forces with oversized bearing clearances were first simulated and later the accelerations on the engine block were calculated using the measured FRFs to the measurement point. The (2D) model of impact force is built in the software Simulink®. Even though it is feasible to model the transfer function from the impact point of the big end bearing to the measurement surface point on the engine block, such as by using a lumped parameter or FE model, for convenience in this paper, the spectra of simulated accelerations were obtained by multiplying the simulated forces and measured transfer functions in the frequency domain. The simulation model involves the interactions between two systems: kinematic/kinetic system and hydrodynamic system. The effect of the lubricating oil was solved using Reynolds equation. The scheme of the interaction between the kinematic/kinetic system and the lubrication system is shown in Figure 8.

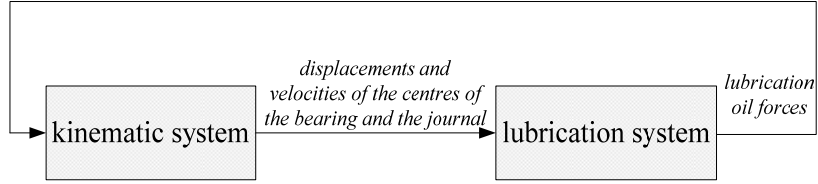


Figure 8. Interaction between kinematic/kinetic system and lubrication system

If an oversized clearance is considered in the big end bearing, the piston and connecting rod can be modelled as one motion subsystem and the crank can be modelled as another motion subsystem. The length from the centre of the small end to the centre of gravity (CG) of the connecting rod is b_1 and the length from the centre of big end to the CG of the connecting rod is b_2 . The friction force on the piston has been considered negligible compared to the combustion force and the vertical inertia force of the piston. The lubricant force in the bearing can be represented by two components: horizontal F_y and vertical F_z (Y horizontal and Z vertical). The forces on the bearing and the journal have the same values but in opposite direction. F_{yc} equals F_{yb} and F_{zc} equals F_{zb} and all of them are the hydrodynamic forces from the lubrication oil. For the modelling of bearing knock faults, the clearance between the piston and the inner wall was ignored, so the piston has no horizontal motion (but there is a horizontal reaction force from the inner wall). The small end bearing connecting the piston and connecting rod was also assumed to be a perfect joint. For the whole system, there are three degrees of freedom: crank angular motion, connecting rod angular motion and the translational motion of the piston in the Z direction. The kinematic equations can be written as:

$$I_c \ddot{\theta} = F_{yc} R \cos \theta + F_{zc} R \sin \theta - T_{fric} - T_{load} \quad (2)$$

$$\begin{bmatrix} m_p + m_b & -b_1 m_b \sin \phi \\ -b_1 m_b \sin \phi & I_b + b_1^2 m_b \end{bmatrix} \begin{bmatrix} \ddot{z}_p \\ \ddot{\phi} \end{bmatrix} + \begin{bmatrix} 0 & -\dot{\phi} b_1 m_b \cos \phi \\ 0 & 0 \end{bmatrix} \begin{bmatrix} \dot{z}_p \\ \dot{\phi} \end{bmatrix} = \begin{bmatrix} F_{zb} - F_g \\ -F_{yb} b \cos \phi - F_{zb} b \sin \phi \end{bmatrix} \quad (3)$$

where I_c is the moment of inertia of the crankshaft (plus flywheel), T_{fric} is the friction and pumping torque of the engine, T_{load} is the external load imposed on the engine, m_p is the mass of the piston and m_b is the mass of the connecting rod and I_b is the moment of inertia of the connecting rod about its CG. \dot{z}_p and \ddot{z}_p are the velocity and acceleration of the piston in the Z direction.

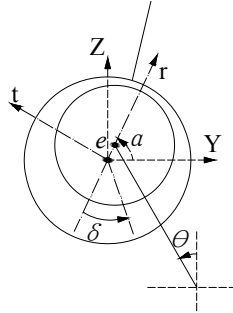


Figure 9. The geometry of the big end bearing

The lubrication force can be solved by Reynolds equation. As shown in Figure 9, there are two coordinate systems. One is the global YZ system and the other is related to the eccentricity line rt system, based on the diameter through the point of minimum oil thickness. α is the coordinate angle between the positive r direction and the positive Y direction. If e is the eccentricity and c is the radial clearance, the eccentricity ratio ε can be calculated as e/c . δ is the angle in the circumferential direction starting from the negative axis of r . The length to diameter ratio of the big end bearings in the engine is smaller than 0.5, so the oil film pressure distribution in the big end bearing can be approximated as a short journal bearing [30]:

$$p = \frac{6\mu c}{h^3} [\dot{\varepsilon} \cos \delta + \varepsilon(\dot{\alpha} - \bar{\omega}) \sin \delta] \left(z^2 - \frac{1}{4} L_b^2 \right) \quad (4)$$

where h is the thickness of the oil film and $h = c(1 + \varepsilon \cos \delta)$. The lubrication force can be integrated about the angle δ . The normal force F_r and tangential F_t can be written as:

$$F_r = - \int_{-L_b/2}^{L_b/2} \int_{\delta_i}^{\delta_o} p R_b \cos \delta d\delta dz \quad (5)$$

$$F_t = - \int_{-L_b/2}^{L_b/2} \int_{\delta_i}^{\delta_o} p R_b \sin \delta d\delta dz \quad (6)$$

where R_b is the radius of the bearing, δ_i is the start angle and δ_o is the end angle of the integration. The Gmbel boundary condition is the most reasonable for the force integration of short journal bearings. Only the positive pressure section is considered and it is assumed there is a π oil film in the bearing. So in the integration, δ_o equals δ_i plus π . Finally the force components in the global YZ coordinates can be derived using the transformation matrix about the angle coordinate α .

As mentioned before, the bearing knock fault can be diagnosed at higher engine speed (3000 rpm) from the change in the squared envelope signal but it is very difficult to detect the faults at lower speeds (1500 rpm and 2000 rpm). During the simulation, the same problem was also encountered. It is very difficult to adjust the model to get agreement between the experimental results and simulated results at lower speeds, so simulation is currently limited to the higher speed condition (3000 rpm). As for the simulation of the piston slap faults in the preceding section, the target of the simulations here is to produce the envelope signals as accurately as possible rather than the raw acceleration signals, so the envelopes of the simulated vibration signals were calculated. An example of the simulated and measured envelopes with a bearing knock fault is shown in Figure 10. It can be seen the simulated envelope signals have a good match with experiment.

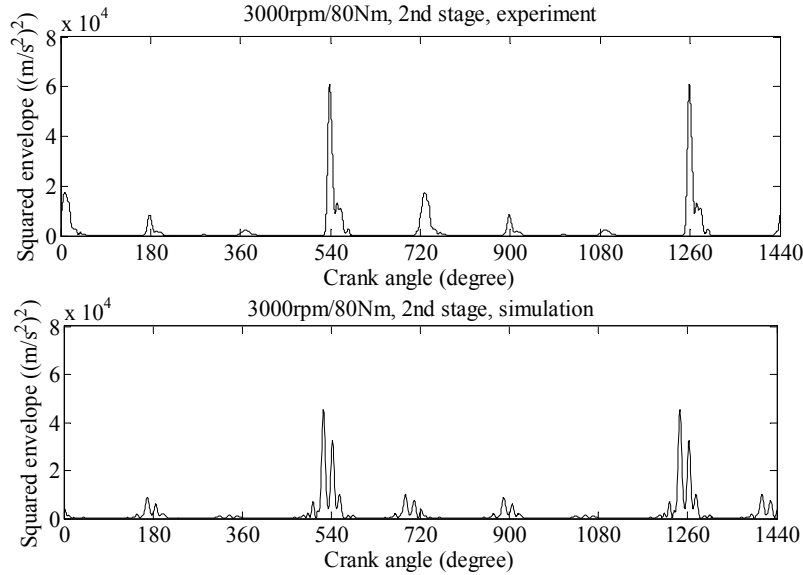


Figure 10. Simulated and experimental envelope signals with the 2nd stage bearing knock fault

5 ANN system

Three-stage network systems were proposed to diagnose and make prognosis of faults in an engine (as shown in Figure 11). The first stage is the fault detection stage where the inputs to the networks are the selected amplitude features of the simulated signals. In the second stage, the neural network localizes which cylinder has faults and the inputs to the network are the selected phase features of the simulated signals. In the third stage, based on the detection and location results, the severity of the faults is identified by the selected amplitude features. The detection stage and severity stage were enacted by MLP (Multi Layer

Perceptron) networks, MLP1 for detection and MLP2 for severity identification. PNNs (Probabilistic Neural Networks) were used to identify which cylinder has faults. The outputs of the PNN are the integer numbers 1, 2, 3 and 4, which directly indicate the cylinder number.

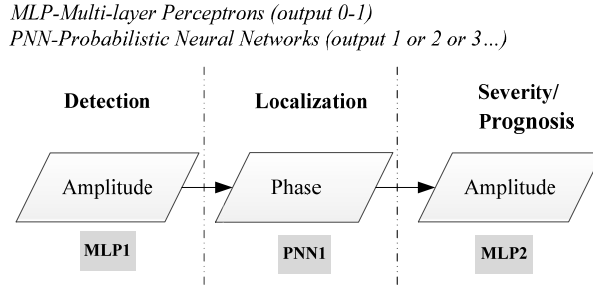


Figure 11: Structure of the three-stage ANN based virtual sensor system

5.1 For misfire diagnosis

For the automated diagnosis system for misfires, there are 120 cases in total, 36 cases from the experiments and the remaining 84 cases from the simulations. The distribution of the different conditions from experiment and simulation is shown in Table 1. The networks were trained using only simulated cases and tested by experimental cases. So in the MLP1, the training group consist of 84 simulated cases and the test group consists of all 36 experimental cases. After the detection stage, the training and test cases for the PNN were reduced to the group of all cases with misfires (misfires in different cylinders). Likewise, the training and test cases for the MLP2 were reduced too, so the severity identification became more specific. As discussed in the preceding sections, the amplitudes of the 1st and 4th harmonics are suitable input features for the MLP1 and MLP2 and the phase of the 1st harmonic for the PNN.

	training group			test group		
	normal	100% misfire	50% misfire	normal	100% misfire	50% misfire
from experiment	9 in total	14 in total, 6 in cylinder 1 6 in cylinder 2 2 in cylinder 3	1 in total, 1 in cylinder 1	6 in total	5 in total, 3 in cylinder 1 1 in cylinder 2 1 in cylinder 3	1 in total, 1 in cylinder 1
from simulation	18 in total	39 in total, 11 in cylinder 1 11 in cylinder 2 9 in cylinder 3 8 in cylinder 4	6 in total, 2 in cylinder 1 2 in cylinder 2 2 in cylinder 3	6 in total	12 in total, 3 in cylinder 1 3 in cylinder 2 3 in cylinder 3 3 in cylinder 4	3 in total, 1 in cylinder 1 1 in cylinder 2 1 in cylinder 3

Table 1: The distribution of data for misfire diagnosis system

A fitness criterion was introduced to evaluate the performance of the MLP1:

$$Error = \frac{1}{N} \sum_{i=1}^N |(ANN(i) - VAL(i))| \quad (7)$$

where, ANN is the output of the MLP and VAL is the corresponding target number. N is the total number of the test group (36). A higher fitness criterion means poorer MLP performance. The trial and error procedure for the number of hidden neurons is also based on the values of fitness criterion.

The final results of the MLPs and the PNN are shown in Table 2. It can be seen that because the pseudo angular acceleration is subject to more complicated influences and is more difficult to simulate, its fitness criteria are worse than those from the torsional vibration method. The final results have also shown that the PNN successfully localized which cylinder has misfire: eight cases in cylinder 1, five cases in cylinder 2,

five cases in cylinder 3 and three cases in cylinder 4. The results in the third column of Table 2 show that the MLP2 also identified the severity of the misfires with reasonable accuracy.

	Detection(MLP1)	Localization(PNN)	Severity (MLP2)	
			100% misfire	50% misfire
Torsional vibration	100% correct error=0.5668	100% correct	output range 0.8747-0.9992	output range 0.5286, 0.4252
Angular acceleration	100% correct error=0.6862	100% correct	output range 0.8488-0.9998	output range 0.4117, 0.409

Table 2: Results of ANNs for misfire diagnosis

5.2 For piston slap fault diagnosis

The simulated signal for a certain speed/load condition is deterministic, but in reality the measurement signals have small deviations in different test scenarios, so a variation in the simulated signals should be instituted to create representative cases for the ANN training. The standard deviation of the variations was set by analysing the normal conditions from experiments and was applied to the simulated enveloped signals. The piston slap faults were also simulated in different cylinders for each speed and load condition and all the simulated signals were instituted with variations.

In the automated diagnosis system for piston slap faults, all training data are from the simulated (squared) envelope signals. The training cases included 288 piston slap faults and 112 cases with normal piston clearance. 49 experimental cases (some of them having combustion faults) were used to test the networks, of which 28 cases are with piston slap faults. For the PNN, the number of training cases is reduced to 288 and the number of test cases is reduced to 28. In the MLP2 of the severity identification stage, the training and test group are reduced to piston slap fault cases for the individual cylinder only. The output of the MLP1 is from 0 to 1; 0 for normal condition, and 1 for fault condition. In the severity identification stage (MLP2), the output 0.5 means three times oversized piston slap faults and 1 means six times oversized piston slap faults. The outputs of MLP1 are shown in Figure 12. In reality, there are piston slap faults for cases 1 to 18 and 33 to 42. The fitness criterion in Equation (7) was also introduced to test the performance of MLP1. The final fitness criterion is 0.2253, so the MPL1 100% correctly detected all piston slap faults.

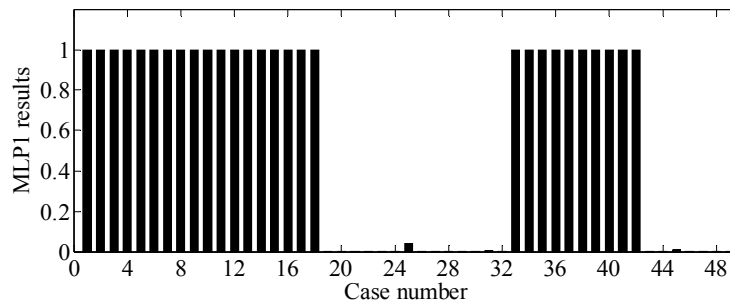


Figure 12: Output of MLP1 for the piston slap faults

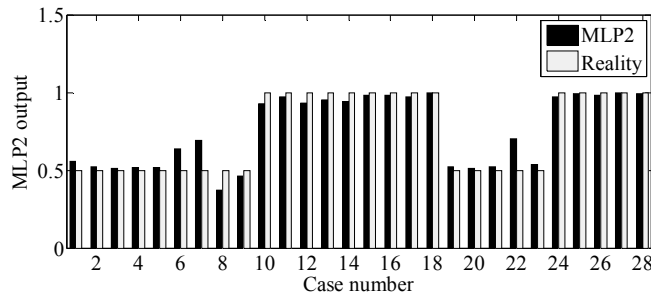


Figure 13: Output of MLP2 for the piston slap faults

For the localization of the piston slap faults, using the selected phase features as inputs, the PNN also achieved a good classification result. The results 100% match with the real situation of the test cases: all piston slap faults (28 cases) occurred in cylinder 1 in the experiments. After the piston slap fault detection stage, the severity identification became more specific. The output results of MLP2 are shown in Figure 13. It can be seen that MLP2 100% correctly identified the severity classification of the piston slap faults with a small deviation. It was also found that the MLP2 need more computing time (more epochs) to achieve the training goal and the final fitness criterion (1.8455) is much larger compared to the MLP1.

5.3 For bearing knock fault diagnosis

As for the other cases, the simulated signal with bearing knock faults is deterministic as well, but in reality the measurement signals have deviations; in particular the transfer function of the bearing knock fault is more complicated. Bearing knock faults were simulated in different cylinders at 3000rpm and three load conditions with both oversized clearances. Variations in the simulated signals were again instituted to create representative cases for the ANN training. As found from the experimental results, the peak values of the squared envelope of the bearing knock faults have no proportional relationship with the load, and they only have very small change at 50Nm, 80Nm and 110Nm.

As before, an MLP was designed for the detection stage (MLP1) and a PNN was developed for the fault localization. Finally another MLP was used for the severity identification (MLP2). In total, 120 cases were used for the training of the MLP1 and all of them are from simulation. 72 training cases are with bearing knock faults and 48 training cases are free from bearing knock faults. 37 cases from real experiments were used to test the MLP1; those from cases 1 to 10 are with bearing knock faults and those from cases 11 to 37 are with normal bearing clearance (but from 32 to 37 are with piston slap faults). The final results of MLP1 are shown in Figure 14. Note that the output of case 37 is 0.3034, but if the threshold of the detection is taken as 0.5, the output would still be considered as free of bearing knock fault. Therefore, the conclusion is that the MLP1 100% correctly detected the bearing knock faults. The fitness criterion in Equation (7) was also used to evaluate the performance of MLP1 and the result is 0.6814. It is noteworthy because only one speed condition was considered in the ANNs of bearing knock faults, but all three speeds and three loads were considered in the ANNs of misfires, the fitness criterion of the MLP1 for the misfire detection is higher than that for the bearing knock faults.

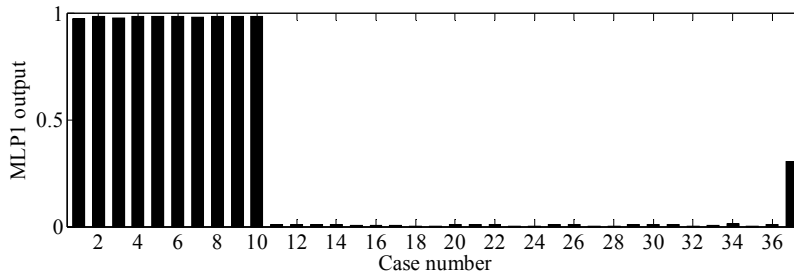


Figure 14: Output of MLP1 for the bearing knock faults

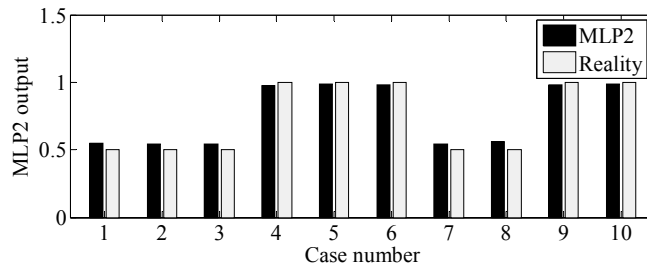


Figure 15. Output of MLP2 for the bearing knock faults

For the PNN, the training cases were reduced to 72 cases (18 cases for each cylinder). 10 cases from real experiments were used to test the PNN of which all are in cylinder 2. The final results show that all

output numbers from the PNN are 2, so the PNN 100% correctly identified which cylinder had bearing knock faults. The output 0.5 of the MLP2 indicates the 1st stage bearing knock faults and the output 1 indicates the 2nd stage bearing knock faults. The output of MLP2 is shown in Figure 15. It can be seen that the MLP2 also got 100% correct results for the severity identification.

6 Conclusions

ANN-based automated systems were separately developed for the diagnosis of misfire, piston slap fault and bearing knock fault in this paper. In order to get sufficient data for training the networks, new simulation models, which can simulate combustion faults and mechanical faults in engines, were developed. The simulation models were updated and optimized by a limited number of tests. Only the simulated data was used to train the networks and the experimental cases were used to test the performance of the networks. Each automated system consists of three stages: MLP1 for the detection stage, PNN for the localization stage and MLP2 for the severity identification stage. The selected amplitude features were used in the detection stage and severity identification stage and the selected phase features were used in the PNNs to localize which cylinder has a fault. For the two misfire diagnosis methods (torsional vibration and pseudo angular acceleration of the engine block), the ratios of the amplitudes of the 1st and 4th harmonics were used for the misfire detection and severity identification, and the phase of the 1st harmonic was used for the misfire localization. Envelope analysis of the vibration signals was applied for the diagnosis of piston slap and bearing knock faults. Compared to the feature selection for the diagnosis of misfire, the feature selection for the diagnosis of the two mechanical faults is more complicated, especially for the selection of the amplitude features. Advanced feature selection methods were applied to select the best amplitude features. The final results have shown that the designed automated systems can efficiently diagnose different fault conditions, including location and severity.

Acknowledgements

The author would like to convey special gratitude to the Australian Research Council and LMS International for sponsoring this research under Linkage Project LP0883486. Part of the research was conducted in the frame of the ITEA 2 project 11004 MODRIO (Model driven physical systems operation). The financial support of the IWT (Flemish Agency for Innovation by Science and Technology) is gratefully acknowledged.

References

- [1] Y. Gao, and R. B. Randall, *Reconstruction of diesel engine cylinder pressure using a time domain smoothing technique*, Mechanical Systems and Signal Processing, vol. 13, no. 5, Academic Press (1999), pp.709-722.
- [2] P. Azzoni, and M. Marseguerra, *Assessment of the potential of a Wiener-Hilbert filter for automatic diagnosis of spark ignition engine faults*, Mechanical Systems and Signal Processing, vol. 9, no. 2, Academic Press (1995), pp. 119-128.
- [3] J. Antoni, J. Daniere, F. Guillet and R.B. Randall, *Effective vibration analysis of IC engines using cyclostationarity. Part II – New results on the reconstruction of the cylinder pressures*, Journal of sound and vibration, vol.257, no.6, University Press (2002), pp. 839-856.
- [4] S. J. Citron, J. E. O'Higgins, and L. Chen, *Cylinder by cylinder engine pressure and pressure torque waveform determination utilizing speed fluctuations*, SAE Press (1989), SAE Paper 890486.
- [5] J. Williams, *An overview of misfiring cylinder engine diagnostic techniques based on crankshaft angular velocity measurements*, SAE Press (1996), SAE Paper 960039.
- [6] J. J. Moskwa, W. Wang, and D. J. Bucheger, *A New Methodology for Engine Diagnostics and Control Utilizing 'Synthetic' Engine Variables: Theoretical and Experimental Results*, Transactions of the ASME: Journal of Dynamic Systems, Measurement, and Control, vol.123, ASME Press (2001), pp.528-534.

- [7] Y. Zhang, and R. B. Randall, *The In-Cylinder Pressure Reconstruction and Indicated Torque Estimation Based on Instantaneous Engine Speed and one Measured In-Cylinder Pressure*, Comadem Conference, Faro, Portugal, 2007, 13-15 June
- [8] M. Desbazeille, R. B. Randall, F. Guillet, M. El Badaoui and C. Hoisnard, *Model-based diagnosis of large diesel engines based on angular speed variations of the crankshaft*, Mechanical Systems and Signal Processing, vol. 24, no.5, Academic Press (2010), pp.1529–1541.
- [9] E. E. Ungar and D. Ross, *Vibration and noise due to piston slap in reciprocating machinery*, Journal of Sound and Vibration, vol.2, no.2, University Press (1965), pp.132–146.
- [10] S. D. Haddad, and P. W. Fortescue, *Simulating Piston Slap by an Analog Computer*, Journal of Sound and Vibration, vol. 52, no.1, University Press (1977), pp.79-93.
- [11] P. D. McFadden and S. R. Turnbull, *Dynamic analysis of piston secondary motion in an internal combustion engine under non-lubricated and fully flooded lubricated conditions*, Proceedings of the Institution of Mechanical Engineers, Part C: Journal of Mechanical Engineering Science, vol.225, SAGE Publications (2011), pp.2575-2585.
- [12] S. H. Cho, S. T. Ahn and Y. H. Kim, *A simple model to estimate the impact force induced by piston slap*, Journal of Sound and Vibration, vol.255, no.2, University Press (2002), pp.229-242.
- [13] A.L. Schwab, J. P. Meijaard and P. Meijers, *A comparison of revolute joint clearance models in the dynamic analysis of rigid and elastic mechanical systems*, Mechanism and Machine Theory, Pergamon Press (2002), vol.37, no.9, pp.895–913.
- [14] P. Flores, J. Ambrósio, J. C. P. Claro, H. M. Lankarani and C. S. Koshy, *Lubricated revolute joints in rigid multibody systems*, Nonlinear Dynamics, vol.56, no.3, Springer Press (2009), pp 277-295.
- [15] G. B. Daniel, K. L. Cavalca, *Analysis of the dynamics of a slider-crank mechanism with hydrodynamic lubrication in the connecting rod-slider joint clearance*, Mechanism and Machine Theory, vol.46, no.10, Pergamon Press (2011), pp.1434–1452.
- [16] Z. Geng and J. Chen, *Investigation into piston-slap-induced vibration for engine condition simulation and monitoring*, Journal of Sound and Vibration, vol.282, no.3-5, University Press (2005), pp.735–751.
- [17] Y. J. Li, P. W. Tse and X. Yang, *EMD-based fault diagnosis for abnormal clearance between contacting components in a diesel engine*, Mechanical Systems and Signal Processing, vol. 24, no. 1, Academic Press (2010), pp.193-210.
- [18] J. N. Chi, *Non-invasive diagnostics of excessive bearing clearance in reciprocating machinery*, MSc Thesis, MIT, USA, 1995
- [19] B. Li, M.Y. Chow, Y. Tipsuwan, J.C. Hung, *Neural-network-based motor rolling bearing fault diagnosis*, IEEE Transactions on Industrial Electronics, vol.47, no.5, IEEE Press (2000), pp.1060-1069.
- [20] B. Samanta and K. R. Al-Balushi, *Artificial neural network based fault diagnostics of rolling element bearings using time domain features*, Mechanical Systems and Signal Processing, vol.17, no.2, Academic Press (2003), pp.317-328.
- [21] V. Crupi, E. Guglielmino and G. Milazzo, *Neural-network-based system for novel fault detection in rotating machinery*, Journal of Vibration and Control, vol.10, no.8, SAGE Publications (2004), pp.1137-1150.
- [22] H. Nahvi and M. Esfahanian, *Fault identification in rotating machinery using artificial neural networks*, Proceedings of the Institution of Mechanical Engineers, Part C: Journal of Mechanical Engineering Science, vol. 219, no.2, SAGE Publications (2005), pp.141-158.
- [23] J. Rafiee, F. Arvani, A. Harifi, and M. H. Sadeghi, *Intelligent condition monitoring of a gearbox using artificial neural network*, Mechanical Systems and Signal Processing, vol. 21, no.4, Academic Press (2007), pp.1746-1754.
- [24] J. Chen and R. B. Randall, *A vibration signal based simulation model for the misfire of internal combustion engines*, 2011 June 20-22nd, CM & MFPT2011, Cardiff, UK
- [25] J. Chen, R. B. Randall, B. Peeters, H. Van der Auweraer, and W. Desmet, *Automated diagnosis of piston slap in engines*, CM & MFPT2012, 2012 June 12-14th, London, UK, 2012
- [26] J. Chen, R. Randall, B. Peeters, H. Van der Auweraer and W. Desmet, *Inertial property estimation by the modal model method*, ISMA 2012, 2012 September 18-20th, Leuven, Belgium
- [27] J. Antoni, *Fast computation of the kurtogram for the detection of transient faults*, Mechanical Systems and Signal Processing, vol.21, no.1, Academic Press (2007), pp.108-124.
- [28] O. Ludwig and U. Nunes, *Novel maximum-margin training algorithms for supervised neural networks*, IEEE Transaction on Neural Networks, vol.21, no.6, IEEE Press (2010), pp.972-983.

- [29] J. Chen, R. Randall, B. Peeters, W. Desmet and H. Van der Auweraer, *Neural network based diagnosis of mechanical faults in IC engines*, IMechE Tenth International Conference on Vibrations in Rotating Machinery, 2012 September 11-13th, London, UK
- [30] O. Pinkus and S. A. Sternlicht, *Theory of Hydrodynamic Lubrication*, McGraw-Hill Press (1961), New York, USA.